Self-Assembly of Rod-Coil Molecules into Lateral Chain-Length-Dependent Supramolecular Organization

Ke-Li Zhong,[1] Qi Wang,[1] Tie Chen,[1,2] Zhegang Huang,[3] Bingzhu Yin,[1] Long Yi Jin[1]

[1]*Key Laboratory for Organism Resources of the Changbai Mountain and Functional Molecules, Ministry of Education, and Department of Chemistry, College of Science, Yanbian University, No. 977 Gongyuan Road, Yanji 133002, People's Republic of China*
[2]*State Key Laboratory of Elemento-organic Chemistry, Nankai University, Tianjin 30071, People's Republic of China*
[3]*Department of Chemistry, Seoul National University, Seoul 151-747, Korea*

Received 31 August 2010; accepted 22 March 2011
DOI 10.1002/app.34555
Published online 9 August 2011 in Wiley Online Library (wileyonlinelibrary.com).

ABSTRACT: In this article, we report synthesis and characterization of the self-assembly behavior of coil-rod-coil molecules, consisting of four biphenyls and a *p*-terphenyl unit linked together with ether bonds as a rod segment. These molecules contain lateral methyl or ethoxymethyl groups at 2 and 5 positions of the middle benzene ring of *p*-terphenyl. The self-assembling behavior of these materials was investigated by means of DSC, POM, and SAXS in the bulk state. The results reveal that self-assembling behavior of these molecules is dramatically influenced by a lateral methyl or ethoxymethyl groups in the middle of rod segment. In addition, molecule with PEO (DP = 17) coil chains of identical coil volume fraction to the corresponding molecule connected by PPO (DP = 12) coil chains, shows diverse self-organizing behavior that may result from the parameters of cross-sectional area of coil segment and the steric hindrance at the rod/coil interface. © 2011 Wiley Periodicals, Inc. J Appl Polym Sci 123: 1007–1014, 2012

Key words: self-assembly; synthesis; SAXS; supramolecular structures; phase behavior

INTRODUCTION

The construction of self-assembling molecular systems with a well-defined size and shape has been widely studied due to their potential applications in areas of molecular electronics, materials science, biomimetic chemistry, and supramolecular chemistry.[1–8] Among self-assembling molecular architectures, rod-coil block molecules provide the spontaneous assemblies of a well-defined supramolecular nanostructures.[9–11] The self-assembling supramolecular structures can be precisely engineered by fine-tuning molecular parameters such as volume fraction of rod to coil segment, the cross-sectional area of coil segment, the shape of rigid rod segment, or molecular shape.[12–15] The molecules self-organize into unique assembling structure from 1-D lamellar, 2-D columnar, discrete bundles to 3-D tetragonal, and so on in the melt, via noncovalent forces including hydrogen bonding, donor-acceptor interactions, electrostatic interactions, hydrophobic and hydrophilic effects, π-π stacking, and reversible ligand-metal interactions.[16–19]

Rod-coil molecules containing lateral chains have a strong tendency to form a 2-D or 3-D aggregation, comparing with no side groups in their molecules. The studies on self-assembly behavior concerning the influence of lateral chains, mostly focused on T-shaped bolaamphiphiles, facial amphiphiles,[20–22] side-chain, or mesogen jacketed polymers,[23–25] Recently, Jin and et al. have reported that a coil-rod-coil oligomer incorporating lateral methyl groups in the center of the rod building block, and poly(propylene oxide) (PPO) coils with the number of repeating units of 17 as coil domain, self-assembles into hexagonal perforated layers aggregation in the melt.[26] More recently, self-assembling behavior of similar coil-rod-coil molecules, incorporating lateral ethyl groups in the center of the rod building block, and poly(ethylene oxide) with a degree of polymerization of 7, 12, and 17 coil segments has been reported by Jin and Hirst groups.[27] In contrast to the

Additional Supporting Information may be found in the online version of this article.

Correspondence to: T. Chen (tchen@ybu.edu.cn) or L. Y. Jin (lyjin@ybu.edu.cn).

Contract grant sponsor: The Program for New Century Excellent Talents in University, Ministry of Education, China.

Contract grant sponsor: The State Key Laboratory of Elemento-organic Chemistry, Nankai University; contract grant number: 201002.

Contract grant sponsor: Jilin Provincial Science and Technology Department; contract grant number: 201115225.

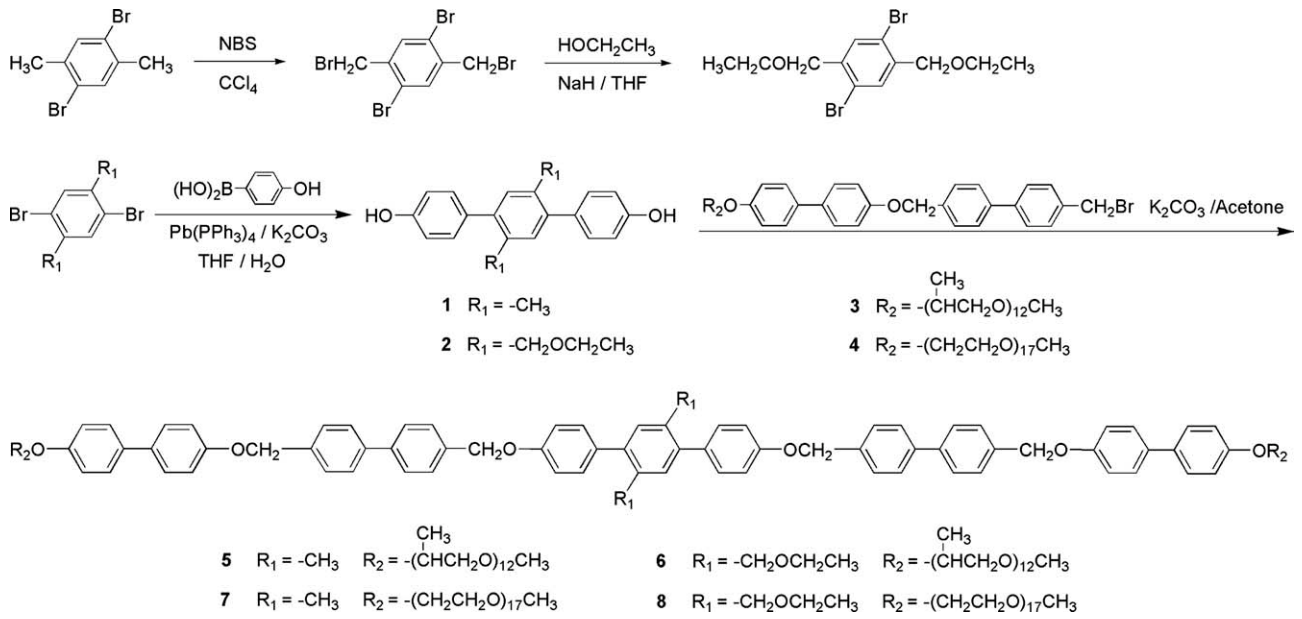

Scheme 1 Synthetic route of rod-coil molecules **5–8**.

molecule without lateral groups at rod segment, the analogous molecules containing lateral methyl or ethyl groups in the center of rod block exhibit an unusual supramolecular structural variation, from lamellar to rectangular structure or form perforated layers to 3-D hexagonal close-packed structure.[26,27] These results imply that the lateral chain of the rod building unit has a strong influence on the creation of the supramolecular structures. Consequently, modification of lateral chain length in the rod segment can provide a novel strategy to manipulate the supramolecular structure for potential applications in biochemistry and materials science.

With this in mind, we have synthesized rod-coil molecules **5–8** (Scheme 1), containing lateral methyl or ethoxymethyl groups in the center of rod segment. The self-assembling behavior of these molecules was investigated by means of differential scanning calorimetry (DSC), thermal polarized optical microscopy (POM), and X-ray diffraction (XRD) in the bulk state.

RESULTS AND DISCUSSION

Synthesis

Rod-coil molecules **5–8**, incorporating of four biphenyls and a *p*-terphenyl unit linked together with ether bonds as a rod segment were synthesized. These molecules consist of poly(propylene oxide) (PPO) with a degree of polymerization (DP) of 12 or poly(ethylene oxide) (PEO) with a DP of 17 as coil segments and contain lateral methyl or ethoxymethyl groups at 2 and 5 positions of the middle benzene ring of *p*-terphenyl. The molecules **5–8** were obtained by substitution reaction of compounds **3** or **4** with 4,4′′-dihydroxyl-2′,5′-dimethyl-*p*-terphenyl (**1**) or 4,4′′-dihydroxyl-2′,5′- di(ethoxymethyl)-*p*-terphenyl (**2**) in the presence of potassium carbonate. The structures of these molecules were characterized by ^{1}H-NMR spectroscopy and a representative analysis of molecules **5** and **8** was shown in Figure 1. The molecular structures of molecules **5–8** were also characterized by matrix-assisted laser desorption ionization time-of-flight (MALDI-TOF) mass spectroscopy and were shown to be in full agreement with the structure presented in Scheme 1 (see Supporting Information).

Structure analysis in the bulk state

The self-assembling behavior of molecules **5–8** was investigated by means of DSC, POM, and XRD in the bulk state. Figure 2 shows the DSC heating and cooling traces of these molecules. The transition temperatures and the corresponding enthalpy changes of molecules **5–8** obtained from DSC heating and cooling scans were summarized in Table I. Molecule **5**, connected with a methyl group at 2 and 5 positions of the middle benzene ring of *p*-terphenyl and poly (propylene oxide) (PPO) with a DP of 12 as coil segments, shows an ordered bulk-state organization with bright birefringence, which transforms into an isotropic liquid at 219.7°C [see Fig. 2(a)]. On slow cooling of molecule **5**, from the isotropic liquid to liquid crystalline mesophase, the focal conical spherulitic fan texture is observed by POM experiment which can preliminarily confirm the presence of an ordered

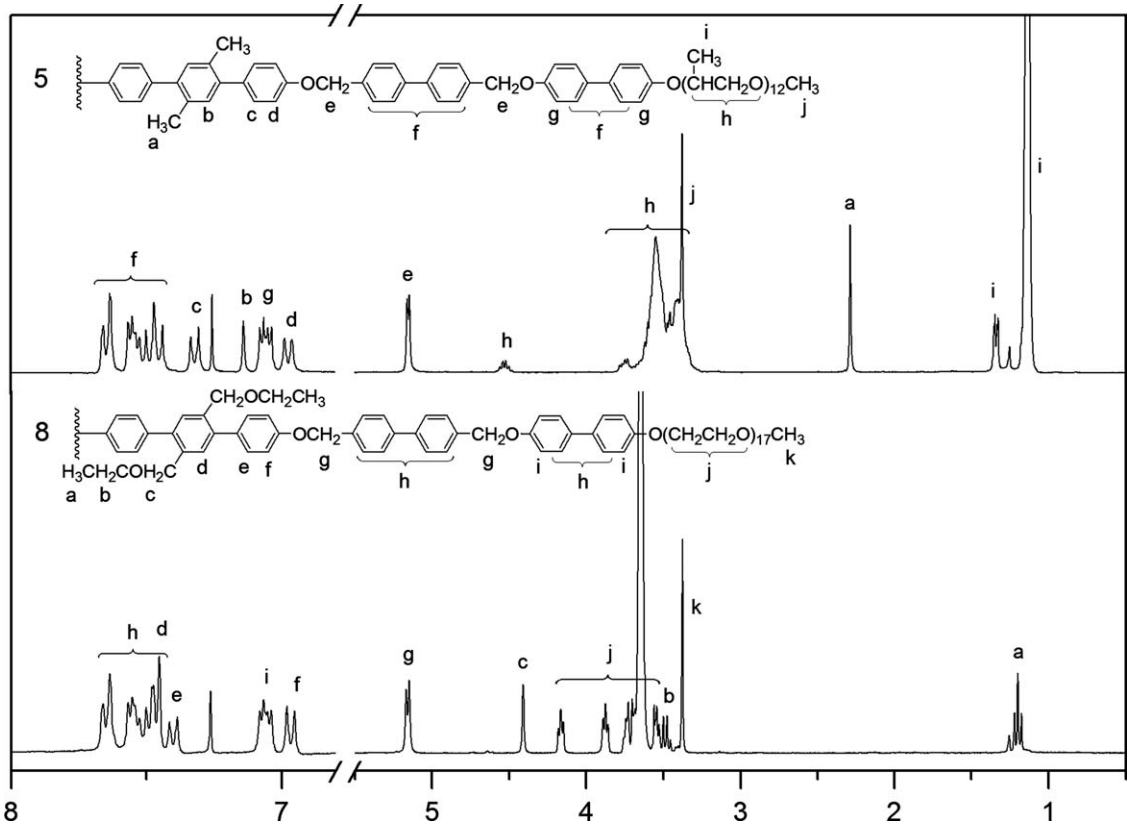

Figure 1 ^{1}H-NMR spectra of molecules **5** and **8** in $CDCl_3$.

columnar phase [Fig. 3(a)]. On further slow cooling to room temperature, a transition to a spherulitic texture with arced striations which are characteristic of a hexagonal perforated lamellar mesophase can be observed [Fig. 3(b)].[28] To confirm the self-assembling structure of molecule **5** in the bulk state, X-ray scattering experiments were performed at various temperatures. Figure 4(a,b) show X-ray diffraction patterns for molecule **5** recorded at 200°C and 25°C on cooling from the isotropic phase to the solid state. The small-angle X-ray scattering (SAXS) diffraction patterns in the liquid crystalline mesophase display several different sharp reflections, which can be assigned as the, (100), (010), (110), (210), and (310) planes for a 2-D oblique columnar structure (*P1* space group symmetry) with lattice parameters $a = 7.07$ nm, $b = 5.71$ nm, and $\gamma = 66°$ [see Fig. 4(a) and Supporting Information Table S1). Wide-angle X-ray scattering (WAXS) data of molecule **5** show only a broad halo centered at approximately 0.48 nm [Fig. 5(a)]. This is indicative of liquid-crystalline like ordering of the aromatic segments within the rod domains. The number of molecules in a single slice of the column, calculated based on the lattice constants and measured densities of molecule **5**, is about 5 [indicating the same number of molecules per columnar cross section irrespective of the length of the PPO chain, see Fig. 6(b)].[13]

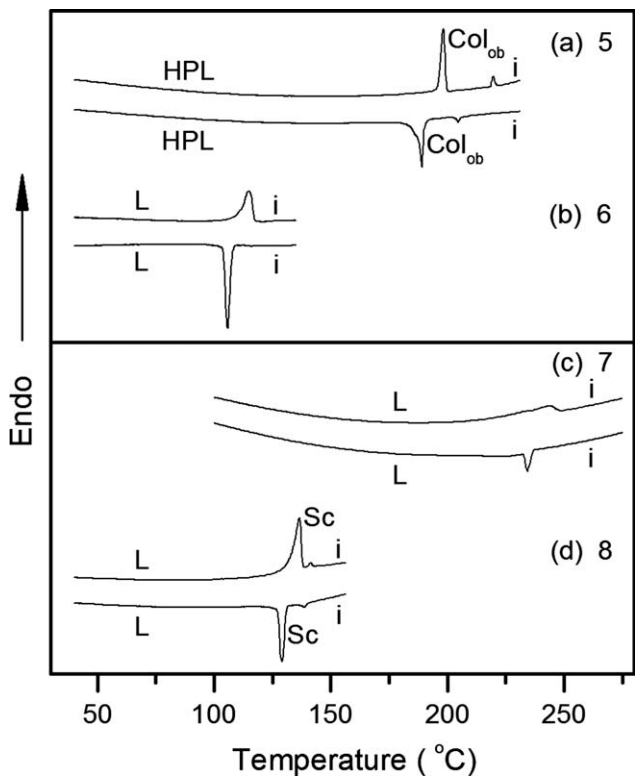

Figure 2 DSC traces (10°C/min) recorded during the heating and the cooling scan of **5–8**.

TABLE I
Thermal Transitions of Molecules 5–8 (Data are from the Second Heating and the First Cooling Scans)

Molecule	f_{coil}	Phase transition (°C) and corresponding enthalpy changes (kJ/mol)	
		Heating	Cooling
5	0.59	HPL 198.2(16.4) Col_{ob} 219.7(1.9) i	i 204.4(1.2) Col_{ob} 189.5(12.6) HPL
6	0.60	L 114.5(20.1) i	i 105.8(28.5) L
7	0.58	L 243.5(10.8) i	i 234.2(11.5) L
8	0.59	L 136.5(17.7) Sc 141.3(1.2) i	i 138.5(0.9) Sc 129.2(15.8) L

f_{coil}, coil volume fraction; L, lamellar; HPL, hexagonal perforated lamellar; Col_{ob}, oblique columnar; Sc, smectic C; i, isotropy.

In the lower temperature crystalline phase, the SAXS diffraction pattern of scattering **5** shows one strong and slight broader reflection, together with four reflections with low intensity at relatively higher angles [Fig. 4(b)]. These reflections can be indexed as the, (100), (002), (110), (103), (004), and (006) planes for a 3-D hexagonal structure ($P\bar{6}m2$ space group symmetry) with lattice parameters $a = 9.0$ nm and $c = 14.5$ nm with $c/a = 1.61$ (see Supporting Information Table S1).[26,28] It should be pointed out that the peak intensity associated with the (002) reflection displays the highest intensity, indicating that the supramolecular 3-D layer structure is composed of an ABAB arrangement crystalline layer of the rod segments with in-plane hexagonal packing of coil perforations [See Fig. 6(a)]. The result of SAXS analysis is consistent with POM experiment.[29] Meanwhile, the WAXS pattern shows three broad peaks at q-spacings of 13.3, 15.7, and 19.3 nm^{-1}, which appear due to crystal packing of the rod segments within the aromatic domain. The molecules pack in a rectangular lattice with unit cell dimensions of $a = 8.0$ Å and $b = 5.8$ Å [See Fig. 5(b)].[13]

Molecule **6,** connected with a ethoxymethyl group at 2 and 5 positions of the middle benzene ring of *p*-terphenyl and poly(propylene oxide) (PPO) with a DP of 12 as coil segments, was synthesized to investigate the chain-length-dependent supramolecular organization. The DSC heating and cooling traces of molecule **6** show the solid phase transforms into an isotropic liquid at 114.5°C [Fig. 2(b)]. SAXS study reveals that molecule **6** self-assembles into a 1-D lamellar aggregation with d spacing 6.58 nm in the crystalline phase [Fig. 4(c)]. Considering molecular length 15.2 nm (by Corey-Pauling-Koltun (CPK) molecular modeling), we confirm that molecule **6** self-organizes into a lamellar structure with the tilted rod domain and the fully interdigitated coil segment [see Fig. 5(c)]. Comparing molecular structures of molecules **5** and **6**, these molecules consist of a same PPO coil segment and have a similar volume fraction ($f_{coil} = 0.59$), while, they incorporate various lateral short-chain-length groups at the 2 and 5 positions of the middle benzene ring of *p*-terpheny unit. Hence, we estimate that the length of the lateral chain remarkably influences on the self-

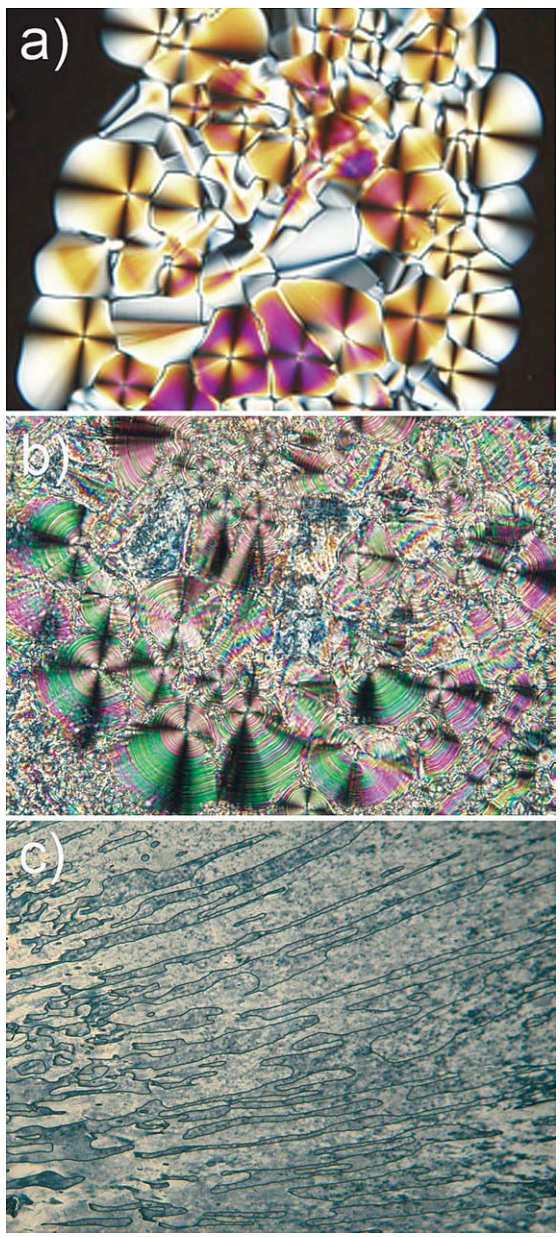

Figure 3 Representative optical polarized micrograph (×100) of the texture exhibited by (a) an oblique columnar structure from the isotropic liquid cooling to the liquid crystalline phase, (b) a hexagonal perforated lamellar structure on cooling to room temperature for molecule **5**, and (c) a smectic C phase for molecule **8** at the transition from the isotropic liquid. [Color figure can be viewed in the online issue, which is available at wileyonlinelibrary.com.]

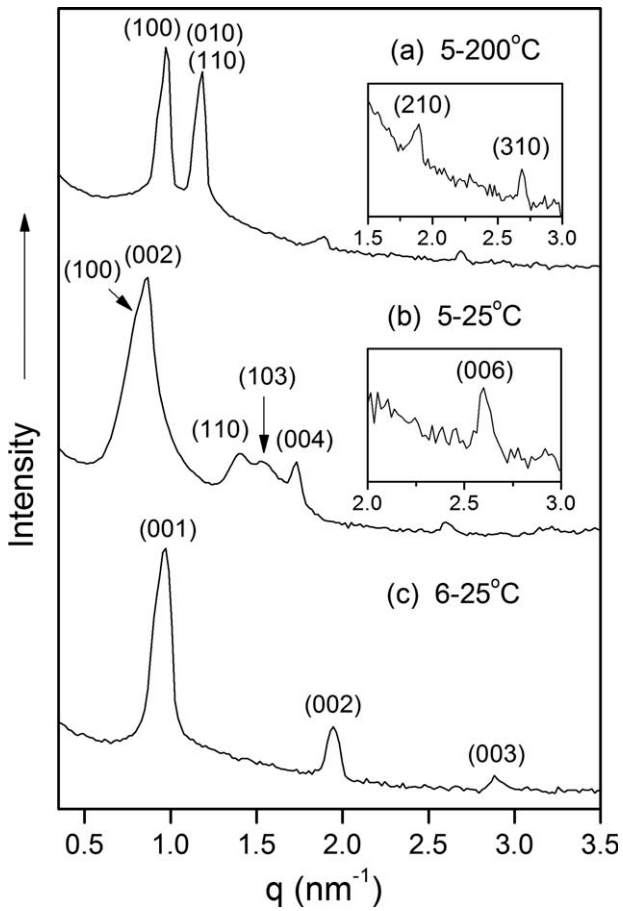

Figure 4 Small-angle X-ray diffraction patterns measured for (a) an oblique columnar structure on cooling to 200°C, (b) a hexagonal perforated lamellar structure at room temperature for molecule **5**, and (c) a lamellar structure at 25°C for molecule **6**.

assembling behavior of rod-coil molecules, based on SAXS study of molecules **5** and **6**. WAXS study of molecules **5** and **6** provide more detailed information of self-organized assemblies. The WAXS patterns shown in Figure 5 exhibit that the rod segment of molecule **5** arrays into a rectangular lattice, however, molecule **6** shows a broad peak in the crystalline phase. These results indicate that the extended lateral chains in the rod segment are able to decrease the molecular interaction of π-π stacking, which lead to loose packing of rod segments and can induce to construct various supramolecular assemblies.

To further study the effect of lateral chain and coil chain length on the self-assembling behaviors of rod-coil molecules, we synthesized molecules **7** and **8**. Molecule **7**, consisting of a methyl group at 2 and 5 positions of the middle benzene ring of *p*-terphenyl and poly(ethylene oxide) (PEO) with a DP of 17 as coil segments, transforms into an isotropic liquid at 243.5°C [Fig. 2(c)]. The self-assembling structure of molecule **7** in the crystalline state was also investigated by X-ray scattering experiment at room temperature. Several peaks in the small-angle region can be indexed as the, (001), (002), and (004) reflections for a 1-D lamellar phase with the layer spacing of 8.17 nm (see Supporting Information Figure S2). Similar to molecule **5**, the WAXS pattern of molecule **7** shows three clear reflections, which can be assigned as the, (110), (200), and (210) planes for a rectangular structure with lattice parameters a = 8.0 Å and b = 5.7 Å [see Fig. 5(d)].

Figure 2(d) shows the DSC heating and cooling traces of molecule **8**, containing two ethoxymethyl groups in the center of rod segment and PEO with a DP of 17 as coil segments. The DSC study shows that a thermotropic liquid crystalline phase of molecule **8** is exhibited at 136.5°C in its melting point and then transfers to the isotropic liquid at 141.3°C. A smectic C mesophase of molecule **8** can be assigned from the POM texture shown in Figure 3(c). The SAXS pattern of molecule **8** shows two equidistant q-spacings peaks for a 1-D lamellar phase at the liquid crystalline state (see Supporting Information Figure S2). The layer spacing of 10.0 nm calculated from 001 plane is smaller than the

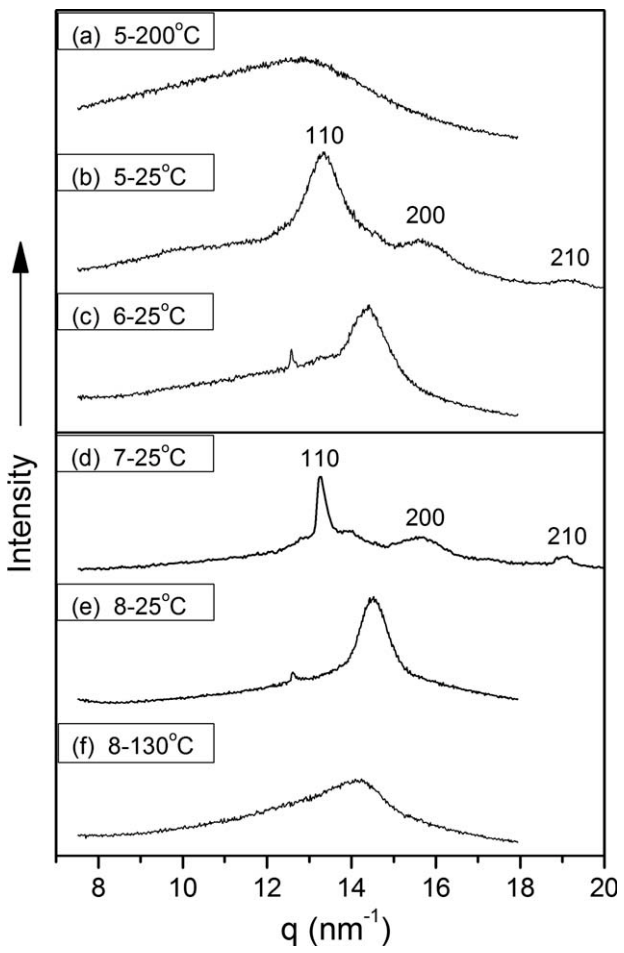

Figure 5 Wide-angle X-ray diffraction patterns of **5–8** in their solid and melt state.

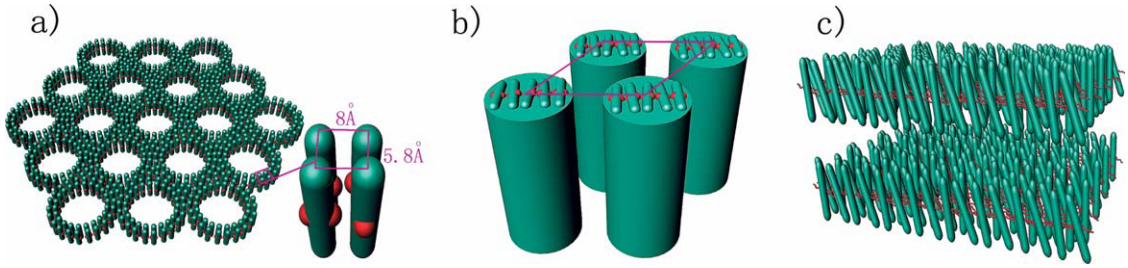

Figure 6 Schematic representation for the formation of (a) hexagonal perforated layer of molecule **5** at solid state, (b) oblique columnar structure of molecule **5** at the liquid crystalline mesophase, and (c) the smectic C phase of molecule **8** in the liquid crystalline phase. [Color figure can be viewed in the online issue, which is available at wileyonlinelibrary.com.]

corresponding estimated molecular length 18.9 nm (by CPK modeling of molecule **8**), further demonstrating the formation of a smectic C phase. While the WAXS pattern shows only a diffuse halo, corresponding to the disordered arrangement of the aromatic rod segments [Fig. 5(f)]. Based upon the data presented so far, a schematic representation of the self-assembled structures of molecules **5–8** is illustrated in Figure 6.

Molecules **7** and **8**, containing the same coil segment (PEO) and similar volume fraction of coil segment form lamellar structure in the crystalline phase. While, molecule **8** connected with two ethoxymethyl groups in the center of rod segment exhibits a smictic C phase in the liquid crystalline phase. This variation of phase behavior is probably caused by the hinderance of the stretch of extended lateral chains, leading to different driving force for packing of the rod segment. It is noteworthy that the different supramolecular nanostructures are constructed by molecules **5** and **7**, which have the same rod segment and equal volume fraction of the coil segment, but have different coil segment. Molecule **5** containing PPO chain exhibits HPL structure and oblique columnar in the solid and liquid crystalline mesophase, respectively. However, molecule **7** containing PEO chains only shows a lamellar structure in the crystalline phase. The variation of self-assembling behavior of these molecules can be explained by different density of the coil/rod interface, and is dependent upon coil cross section. These results imply that the steric hindrance at the rod/coil interface is also one of parameters governing supramolecular rod assembly in coil-rod-coil systems.[30]

CONCLUSIONS

Rod-coil molecules **5–8** consisting of four biphenyls and a *p*-terphenyl, which contains lateral methyl or ethyloxylmethyl groups at 2 and 5 positions of the middle benzene ring were successfully synthesized. These moleucles self-assemble into various supramolecular nanostructures such as, HPL, oblique columnar, and layer structure as a function of lateral chain length of rod-coil molecules. The results reveal that self-assembly of rods can be fine-tuned in the rod-coil system, since, in addition to coil volume fraction, rod anisotropy and the shape of rigid rod segment, the lateral chain length, or coil cross-sectional area is an independent parameter to build a variety of supramolecular structures.

EXPERIMENTAL

Materials

poly(propylene glycol) (M_w = 725), poly(ethylene glycol) methyl ether (M_w = 750), cuprous iodide, 1,4-dibromo-2,5-dimethylbenzene, tetrakis(triphenylphosphine) palladium(0), 4-hydroxyphenylboronic acid (all from Aldrich) and conventional reagents were used as received. 1,4-dibromo-2,5-bis(bromomethyl)benzene, 1,4-dibromo-2,5-bis(ethoxymethyl)-benzene and molecules **1–4** were prepared according to the procedures described elsewhere (see Supporting Information).

Techniques

^{1}H-NMR spectra were recorded from $CDCl_3$ solutions on a Bruker AM 300 spectrometer. A Perkin–Elmer Pyris Diamond differential scanning calorimeter was used to determine the thermal transitions, which were reported as the maxima and minima of their endothermic or exothermic peaks, the heating and cooling rates were controlled to 10°C/min. X-ray scattering measurements were performed in transmission mode with synchrotron radiation at the 5C2 X-ray beam line at Pohang Accelerator Laboratory, Korea. A Nikon Optiphot 2-pol optical polarized microscope, equipped with a Mettler FP82 hot-stage and a Mettler FP90 central

processor, was used to observe the thermal transitions and to analyze the anisotropic texture. MALDI-TOF-MS was performed on a perceptive Biosystems Voyager-DE STR using a 2-cyano-3-(4-hydroxyphenyl) acrylic acid (CHCA) as matrix.

Synthesis of rod-coil molecules 5–8

Coil-rod-coil molecules **5–8** were synthesized using the same procedure. A representative example is described for molecule **5**. Compound **1** (49 mg, 0.17 mmol), compound **4** (432 mg, 0.37 mmol) and K_2CO_3 (230 mg,1.7 mmol) were dissolved in 30 mL acetone. The mixture was refluxed for 36 h, then the solvent was removed and the residue was washed with water. The mixture was extracted with ethyl acetate and the crude product was purified by column chromatography (silica gel, CH_2Cl_2/CH_3OH = 10/1 as eluent). The product was further purified by recycle gel permeation chromatography (JAI) to yield white solid 140 mg (34%).

Compound 5 ^{1}H-NMR (300 MHz, $CDCl_3$, δ, ppm) 7.44-7.66 (m, 24Ar—H, *o* to OCH_2*phenyl*, *m* to OCH_2-*phenyl*, *o* to CH_2Br, *m* to CH_2Br, *m* to CH_2O*phenyl* and *m* to *phenyl*$OCH(CH_3)CH_2O$), 7.31 (d,4ArH, H_2, H_6, $H_{2''}$, $H_{6''}$ of *p*-terphenyl), 7.14 (s,2ArH, $H_{3'}$, $H_{6'}$ of *p*-terphenyl), 7.04–7.08 (dd, 8Ar—H, *o* to CH_2O-*phenyl*, *o* to *phenyl*$OCH(CH_3)CH_2O$), 6.98 (d,4ArH, H_3, H_5, $H_{3''}$,$H_{5''}$ of *p*-terphenyl), 5.15 (d, 8H, phOCH_2ph), 4.52 (m, 2H, ph$OCH(CH_3)CH_2O$), 3.74 (t, 4H, ph$OCH(CH_3)$ CH_2O), 3.37–3.61(m, 72H, —$OCH(CH_3)CH_2O$— and OCH_3), 2.28 (s,6H, phCH_3), 1.34 (d,6H,—$OCH(CH_3)CH_2O$—), 1.13 (d,66H, —$OCH(CH_3)CH_2O$—). MALDI-TOF-MS *m/z* $(M)^+$ 2439, $(M + Na)^+$ 2462.

Compound 6 Yield 50%.^{1}H-NMR (300 MHz, $CDCl_3$, δ, ppm) 7.44–7.66(m, 26Ar—H, *o* to OCH_2-*phenyl*, *m* to OCH_2*phenyl*, *o* to CH_2Br, *m* to CH_2Br, *m* to CH_2O*phenyl*, *m* to *phenyl*$OCH(CH_3)$-CH_2O and $H_{3'}$, $H_{6'}$ of *p*-terphenyl), 7.40(d,4ArH, H_2, H_6, $H_{2''}$, $H_{6''}$ of *p*-terphenyl), 7.04–7.08(dd, 8Ar—H, *o* to CH_2O*phenyl*, *o* to *phenyl*$OCH(CH_3)$-CH_2O), 6.98(d,4ArH, H_3, H_5, $H_{3''}$, $H_{5''}$ of *p*-terphenyl), 5.15(d, 8H, phOCH_2ph), 4.53(m, 2H, ph$OCH(CH_3)CH_2O$), 4.41(s, 4H, phCH_2O),3.74(t, 4H, ph$OCH(CH_3)$ CH_2O), 3.38–3.55(m, 76H, —$OCH(CH_3)CH_2O$—, phOCH_2CH_3 and OCH_3), 1.34(d,6H,—$OCH(CH_3)$ CH_2O—), 1.13–1.25(d,72H, —$OCH(CH_3)CH_2O$—, phOCH_2CH_3). MALDI-TOF-MS *m/z* $(M)^+$ 2527, $(M + Na)^+$ 2550.

Compound 7 Yield 56%.^{1}H-NMR (300 MHz, $CDCl_3$, δ, ppm) 7.45–7.65(m, 24 Ar—H, *o* to OCH_2-*phenyl*, *m* to OCH_2*phenyl*, *o* to CH_2Br, *m* to CH_2Br, *m* to CH_2O*phenyl* and *m* to *phenyl*$OCH(CH_3)CH_2O$), 7.28(d,4ArH, $H_{2,6}$, $H_{2''}$, $H_{6''}$ of *p*-terphenyl), 7.14(s,2ArH, $H_{3'}$, $H_{6'}$ of *p*-terphenyl),7.04–7.08(dd, 8Ar—H, *o* to CH_2O*phenyl*, *o* to *phenyl*$OCH(CH_3)$-CH_2O), 6.97(d,4ArH, H_3, H_5, $H_{3''}$, $H_{5''}$ of *p*-terphenyl), 5.15(d, 8H, phOCH_2ph),4.16(t, 4H, phenyl-OCH_2CH_2O), 3.87(t, 4H, phenylOCH_2CH_2O), 3.53–3.72(m, 128H, —OCH_2 CH_2O—), 3.37(s, 6H, OCH_3), 2.28(s,6H, phCH_3). MALDI-TOF-MS *m/z* $(M)^+$ 2543, $(M + Na)^+$ 2566.

Compound 8 Yield 52%. ^{1}H-NMR (300 MHz, $CDCl_3$, δ, ppm) 7.45–7.66(m, 26Ar—H, *o* to OCH_2-*phenyl*, *m* to OCH_2*phenyl*, *o* to CH_2Br, *m* to CH_2Br, *m* to CH_2O*phenyl*, *m* to *phenyl*$OCH(CH_3)CH_2O$, and $H_{3'}$, $H_{6'}$ of *p*-terphenyl), 7.39(d,4ArH, H_2, H_6H, $_{2''}$, $H_{6''}$ of *p*-terphenyl), 7.04–7.08(dd, 8Ar—H, *o* to CH_2O*phenyl*, *o* to *phenyl*$OCH(CH_3)CH_2O$), 6.97(d,4ArH, H_3, H_5, $H_{3''}$, $H_{5''}$ of *p*-terphenyl), 5.15(d, 8H, phOCH_2ph), 4.41(s, 4H, phCH_2O), 4.16(t, 4H, phenylOCH_2CH_2O), 3.88(t, 4H, phenylOCH_2CH_2O), 3.56–3.65(m, 128H, —OCH_2CH_2O—),3.39(q,4H, phOCH_2CH_3), 3.14(s, 6H, OCH_3), 1.20(t,6H, phOCH_2CH_3). MALDI-TOF-MS *m/z* $(M)^+$ 2645, $(M + Na)^+$ 2668.

We are grateful to Institute of High Energy Physics Chinese Academy of Sciences and Pohang Accelarator Laboratory, Korea for using Synchrotron Radiation Source.

References

1. Rosen, B. M.; Wilson, C. J.; Wilson, D. A.; Peterca, M.; Imam, M. R.; Percec, V. Chem Rev 2009, 109, 6275.
2. Vriezema, D. M.; Aragones, M. C.; Elemans, J. A. A. W.; Cornelissen, J. J. L. M.; Rowan, A. E.; Nolte, R. J. M. Chem Rev 2005, 105, 1445.
3. Ryu, J.-H.; Hong, D.-J.; Lee, M. Chem Commun 2008, 1043.
4. Saez, I. M.; Goodby, J. W. J Mater Chem 2005, 15, 26.
5. Jin, W.; Fukushima, T.; Kosaka, A.; Niki, M.; Ishii, N.; Aida, T. J Am Chem Soc 2008, 127, 8284.
6. Minich, E. A.; Nowak, A. P.; Deming, T. J.; Pochan, D. J. Polymer 1951 2004, 45.
7. Klok, H.-A.; Lecommandoux, S. Adv Mater 2001, 13, 1217.
8. Ariga, K.; Hill, J. P.; Lee, M. V.; Vinu, A.; Charvet, R.; Acharya, S. Sci Technol Adv Mater 2008, 9, 014109.
9. Boer, B. D.; Stalmach, U.; Hutten, P. F.; Melzer, C.; Krasnikov, V. V.; Hadziioannou, G. Polymer 2001, 42, 9097.
10. Olsen, B. D.; Segalman, R. A. Mater Sci Eng R 2008, 62, 37.
11. Cho, B. K.; Lee, M.; Oh, N. K.; Zin, W. C. J Am Chem Soc 2001, 123, 9677.
12. Lee, M.; Cho, B. K.; Zin, W. C. Chem Rev 2001, 101, 3869.
13. Zhong, K. L.; Huang, Z.; Man, Z.; Jin, L.Y.; Yin, B.; Lee, M. J Polym Sci Part A: Polym Chem 2010, 48, 1415.
14. Moore, J. S. Acc Chem Res 1997, 30, 402.
15. Northrop, B. H.; Yang, H.-B.; Stang, P. J. Chem Commun 2008, 5896.
16. Palmer, L. C.; Stupp, S. I. Acc Chem Res 2008, 41, 1674.
17. Ryu, J.-H.; Cho, B.-K.; Lee, M. Bull Kor Chem Soc 2006, 27, 1270.
18. Zhong, K. L.; Chen, T.; Yin, B.; Jin, L. Y. Macromol Res 2009, 17, 280.
19. Zhong, K. L.; Man, Z.; Huang, Z.; Chen, T.; Yin, B.; Jin, L. Y. Polym Int 2011, 60, 845.
20. Tschierske, C. Chem Roc Rev 1930 2007, 36.
21. Horsch, M. A.; Zhang, Z.; Glotzer, S. C. Nano Lett 2006, 6, 2406.

22. Liu, F.; Chen, B.; Glettner, B.; Prehm, M.; Das, M. K.; Baumeister, U.; Zeng, X.; Ungar, G.; Tschierske, C. J Am Chem Soc 2008, 130, 9666.
23. Chen, X.-F.; Shen, Z.; Wan, X.-H.; Fan, X.-H.; Chen, E.-Q.; Ma, Y.; Zhou, Q.; Chem Soc Rev 2010, 39, 3072.
24. Murali, M.; Sudhakar, P.; Satish Kumar, B.; Samui, A. B. J Appl Polym Sci 2009, 111, 2562.
25. Ho, M.-S.; Hsu, C.-S. J Polym Sci Part A: Polym Chem 2009, 47, 6596.
26. Jin, L. Y.; Bae, J.; Ahn, J. H.; Lee, M. Chem Commun 2005, 9, 1197.
27. Tian, L.; Zhong, K.-L.; Liu, Y.; Huang, Z.; Jin, L. Y.; Hirst, L. S. Soft Matter 2010, 6, 5993.
28. Zhong, K. L.; Yang, C.; Huang, Z.; Lee, E.; Chen, T.; Yin, B.; Jin, L.Y. Macromol Res 2010, 18, 289.
29. Jin, L. Y.; Ahn, J. H.; Lee, M. J Am Chem Soc 2004, 126, 12208.
30. Chen, L.; Zhong, K.; Jin, L. Y.; Huang, Z.; Liu, L.; Hirst, L. S. Macromol Res 2010, 18, 800.